2 Physics Goals and Design Drivers

2.1 Quasi-Elastic Scattering

2.1.1 Introduction

Quasi-elastic scattering dominates the total ν–N interaction rate in the threshold regime $E_\nu \leq 2$ GeV. Precision measurement of the cross-section for this reaction, including its energy dependence and variation with target nuclei, is essential to current and future neutrino-oscillation experiments.

2.1.2 Nucleon Form-factors in Quasi-elastic Scattering

MINERνA's large quasi-elastic samples will probe the Q^2 response of the weak nucleon current with unprecedented accuracy. The underlying V-A structure of this current includes vector and axial-vector form-factors. The essential formalism is given in reference [1].

$$< p(p_2)|J^+_\lambda|n(p_1) >= \overline{u}(p_2)\left[\gamma_\lambda F_V^1(q^2) + \frac{i\sigma_{\lambda\nu}q^\nu \xi F_V^2(q^2)}{2M} + \gamma_\lambda\gamma_5 F_A(q^2)\right]u(p_1),$$

where $q = k_\nu - k_\mu$, $\xi = (\mu_p - 1) - \mu_n$, and $M = (m_p + m_n)/2$. Here, μ_p and μ_n are the proton and neutron magnetic moments. The pseudoscalar form-factor is not shown since it is small for ν_μ.

The vector part of this matrix element can be expressed using $G_E^p(q^2)$, $G_E^n(q^2)$, $G_M^p(q^2)$, and $G_M^n(q^2)$. It has been generally assumed that the q^2 dependence of these form-factors can be described by the dipole approximation:

$$G_D(q^2) = \frac{1}{\left(1 - \frac{q^2}{M_V^2}\right)^2}, \;\; M_V^2 = 0.71 \text{ (GeV/c)}^2, \;\; F_A(q^2) = \frac{g_A}{\left(1 - \frac{q^2}{M_A^2}\right)^2}$$

$$G_E^p = G_D(q^2), \quad G_E^n = 0, \quad G_M^p = \mu_p G_D(q^2), \quad G_M^n = \mu_n G_D(q^2).$$

As discussed below, the dipole parameterization is far from perfect. MINERνA will be able to measure deviations of F_A from this form. In general, the axial form-factor $F_A(q^2)$ can only be extracted from quasi-elastic neutrino scattering.[1]

2.1.3 Vector form-factors

Electron scattering experiments at SLAC and Jefferson Lab (JLab) have measured the proton and neutron electromagnetic (vector) form-factors with high precision. The vector form-factors can be determined from electron scattering cross-sections using the standard Rosenbluth separation technique[2], which is sensitive to (two-photon) radiative corrections, or from polarization measurements using the newer polarization transfer technique[3]. Polarization measurements do not directly measure form-factors, but rather the ratio G_E/G_M. Recently, discrepancies in electron scattering measurements of some vector form-factors have appeared; study of quasi-elastic reactions in MINERνA may help reveal the origin these discrepancies. Figure 1 shows the BBBA-2005 (Bradford, Bodek, Budd, Arrington 2005) fits. There appears to be a difference between the two methods of measuring this ratio. The

[1] At low Q^2, below 0.1 (GeV/c)^2, its behavior can also be inferred from pion electroproduction data.

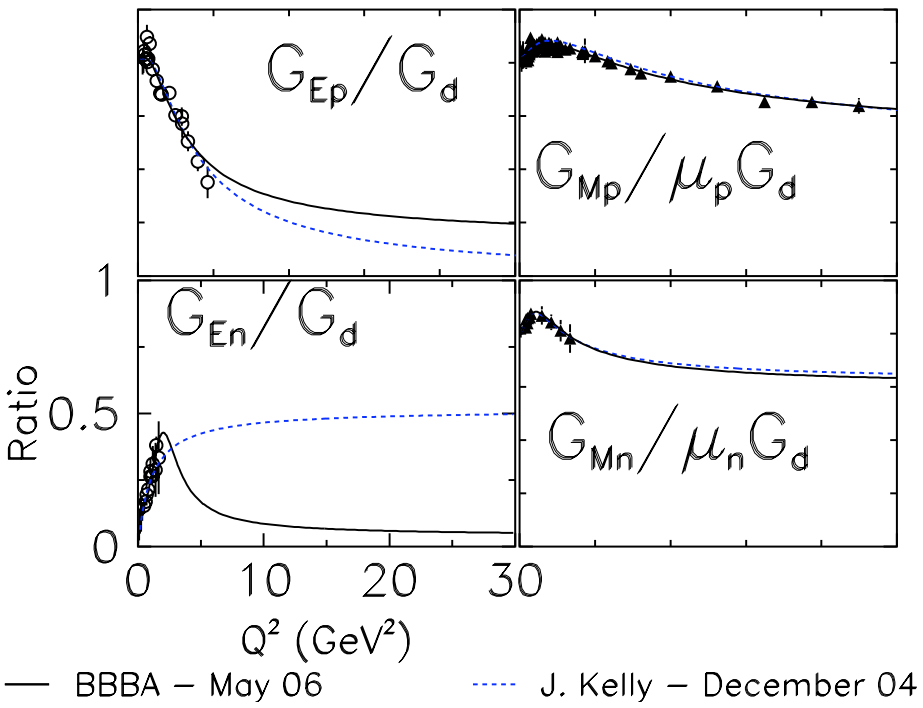

Figure 1: Deviations from dipole approximation are illustrated for two different nucleon form factor parameterizations - J. Kelly [4](dashed Blue) and BBBA05 [5] (solid black). Data are taken from [4].

newer polarization transfer technique yields a much lower value at high Q^2 and indicates a difference between the electric charge and magnetization distributions. The polarization transfer technique is believed to be more reliable and less sensitive to radiative effects from two-photon corrections. In addition, Figure 1 shows that dipole amplitudes provide only a first-order description of form-factor behavior at high Q^2.

If the electric charge and magnetization distributions of the proton are indeed different, accurate measurement of the axial form-factor's high-Q^2 shape in MINERνA can provide important new input to help resolve differences in electron scattering data.

To obtain the correct neutrino cross-sections [6], the input form-factors must be correct. The Q^2 distribution measured in neutrino scattering is sensitive to both the vector and axial form-factors. However, using an incorrect *axial* form-factor to match the the Q^2 distribution in neutrino scattering (to compensate for old dipole *vector* form-factors) results in a 6–8% error in the calculated neutrino cross-section. Therefore, updated vector form-factors *and* better-measured axial form-factors are required. MINERνA will measure the Q^2 dependence of F_A in neutrino scattering and compare the calculated cross-section with the measured cross-section.

2.1.4 Axial form-factor

Neutrino scattering provides the only practical route to precision measurement of the axial form-factor above $Q^2 = 0$, and the functional form of $F_A(Q^2)$. The fall-off of the form-factor strength with increasing Q^2 is traditionally parameterized (approximately) using an effective axial-vector mass M_A. Uncertainty in the value of M_A contributes directly to uncertainty in the total quasi-elastic cross-section. Earlier neutrino measurements, mostly bubble-chamber experiments on deuterium, extracted M_A using the best vector form-factors, other parameters, and models available at the time. Changing these input assumptions changes the extracted value of M_A. Hence, precision extractions of M_A and F_A require using the best possible vector form-factors and coupling constants. The value of M_A is ≈ 1.00 GeV/c^2, to an accuracy of perhaps 5%. This value agrees with the theoretically-corrected value from pion electroproduction[8], 1.014 ± 0.016 GeV/c^2.

The fractional contributions of F_A, G_M^p, G_M^n, G_E^p, and G_E^n to the Q^2 distribution for quasi-elastic neutrino and anti-neutrino scattering cross-sections in energy range of the NuMI beam are shown in Figure 2. The contributions are determined by comparing the BBA-2003 [6] cross-sections with and without each of the form-factors included. MINERνA will be the first systematic study of F_A, which accounts for roughly half of the quasi-elastic cross-section, over the entire range of Q^2 shown in the figure.

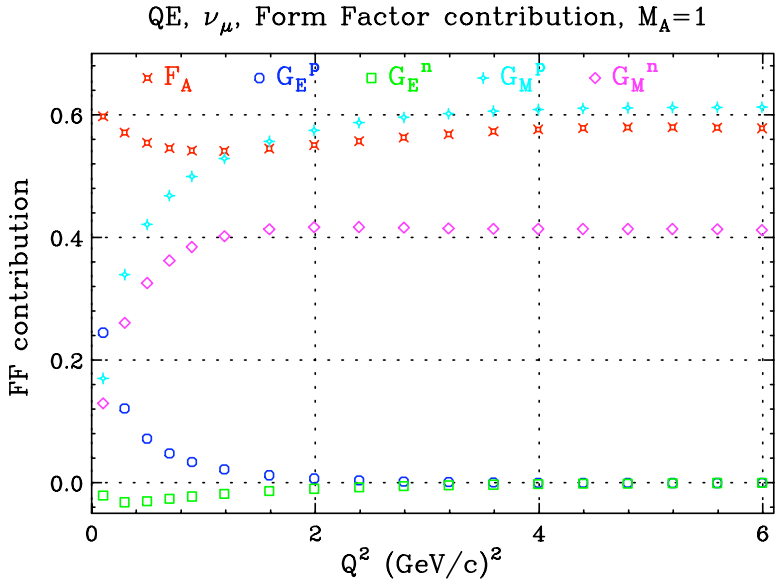

Figure 2: Fractional contributions of G_M^p, G_M^n, G_E^p, G_E^n, and F_A to the Q^2 distributions for quasi-elastic neutrino samples in the energy range of the NuMI beam. Because of interference terms, the sum of the fractions does not necessarily add up to 100%.

2.1.5 Physics of vector and axial form-factors

In deep-inelastic charged-current scattering from quarks, the vector and axial couplings are equal (V-A). Similarly, in electron scattering from quarks (vector current), there is a well-defined ratio between electric and magnetic scattering from point-like Dirac quarks. At low momentum transfers, all of these

relations break down. For example in quasielastic and resonant production at very low momentum transfers, the charge and anomalous magnetic moments of the neutron and proton mean the ratio of electric and magnetic scattering for the vector current is not the same as for free quarks. Similarly, from neutron decay, we know that $g_a(Q^2 = 0) = 1.267$ instead of 1.0, so vector and axial scattering differ at $Q^2 = 0$.

There are efforts in progress by lattice gauge programs to calculate the anomalous vector and axial magnetic moments of the proton and neutron, and the Q^2 dependence of all the form-factors in the low- and high-Q^2 regions. The normalization of the magnetic form-factors at Q^2=0 are constrained to equal the charge and anomalous (vector and axial) magnetic moment. The slope at low Q^2 is related to the mean square charge radius of the proton and neutron. The dipole form assumes that the charge and magnetization distributions of the various types of quarks and antiquarks have an exponential form. For Q^2 above 0.5–1.0 (GeV/c)^2 this non-relativistic picture breaks down. The ratio $G_E/\mu G_M \approx 1.0$ (at low Q^2) implies that the charge and magnetization distribution of the proton are the same, but at higher Q^2 the ratio becomes much smaller, and more sophisticated models are required (e.g. lattice gauge theories). Therefore, measurement of the axial form-factor over a wide range of Q^2 is of great interest. In this section, we show MINERνA's sensitivity to three different models of the axial form-factor:

- Model 1: A simple dipole approximation currently used for the magnetic form-factor of the proton, with different axial and vector radii. This is the current standard assumption.
- Model 2: A constitutuent quark model preformed by Wagenbrunn *et al.*[7].
- Model 3: A model based on duality, which requires the axial and vector parts of $W_1^{elastic}$ to be equal above Q^2=0.5 (GeV/c)^2, and therefore increase with Q^2, as described briefly in the next section.

2.1.6 Quark/hadron and local duality

In modern language, the concept of quark-hadron duality can be related to the momentum sum rule in QCD, and various other moments of the structure functions. It has been shown by Bodek and Yang that with inclusion of target mass corrections, NNLO QCD describes deep-inelastic scattering and the average resonant cross-section down to $Q^2 = 0.5$ (GeV/c)^2. The concept of local duality implies that the integral of the QCD predictions (including target mass) in the threshold region up to pion threshold, should be equal to the integral of the elastic peak. Since for QCD, the vector and axial contributions to W_1 and W_2 are equal, local duality predicts that vector and axial part of the quasi-elastic form-factors should become equal around $Q^2 = 0.5$ (GeV/c)^2. This means that the dipole approximation must break down for both vector and axial form-factors.

The vector and axial components of $W_1^{elastic}$ become equal at $Q^2 \sim 0.5$ (GeV/c)^2 for both BBA and dipole form-factors. The requirement that this vector/axial ratio remains equal to 1.0 for higher Q^2 yields a definite prediction that the axial form-factor is 1.4 times larger than the dipole prediction at higher Q^2.

2.1.7 Axial form-factor measurement in MINERνA

Figure 3 shows a typical quasi-elastic event, as simulated in MINERνA.

In $\nu n \to \mu^- p$, the outgoing proton carries kinetic energy of approximately $Q^2/2M_N$. So for low Q^2, the challenge is identifying events with a very soft recoil proton; for high Q^2, this proton is high

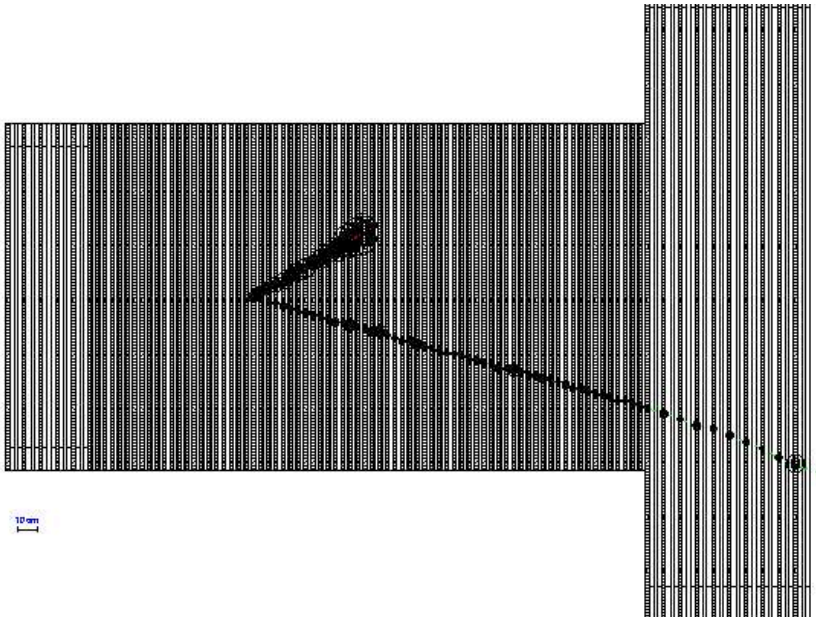

Figure 3: A simulated charged-current quasi-elastic interaction in MINERνA. The proton (upper) and muon (lower) tracks are well resolved. In this display, hit size is proportional to energy loss within a strip. The increased energy loss of the proton as it slows and stops is clear. For clarity the outer detector is not drawn.

energy and may interact in the detector, making particle identification more challenging. The main strategies of the current analysis are:

- At low Q^2, accept quasi-elastic candidates with a single (muon) track, and discriminate from background by requiring low activity in the remainder of the detector
- At higher Q^2, reconstruct both the proton and the muon, and require kinematic consistency with $x = 1$ and $p_T^{tot} = 0$

Simple cuts based on these ideas yield reasonable efficiency and good purity, even at high Q^2.

This analysis uses the NEUGEN generator and the hit-level MINERνA detector simulation and tracking package to model signal selection and background processes.

Initial event identification requires one or two tracks in the active target. One of these tracks must be long range (400 g/cm^2) as expected for a muon. If a second track forms a vertex with this track, it is assumed to be the proton. No other tracks may be associated with this vertex. The muon track momentum is reconstructed with a fractional uncertainty of 10–20%.

For low Q^2, the proton track (if found) is effectively required to lose energy by dE/dx alone, since only limited detector activity not associated with the primary tracks is allowed by the selection criteria. We attempt to recover some of the resulting efficiency loss by allowing hits on tracks near the proton track to be associated with it. Figure 4 shows the fraction of hits not associated with the lepton or proton in the quasi-elastic events and in expected background processes. For higher-Q^2 events a similar procedure could be applied, but it is not particularly effective nor efficient.

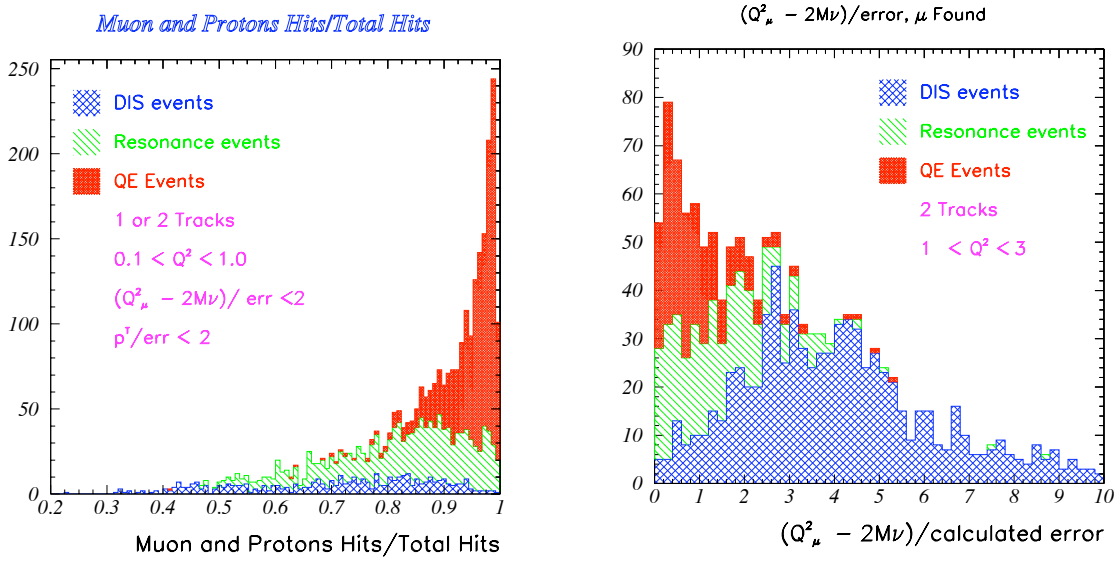

Figure 4: Left: The fraction of hits associated with the muon and the proton tracks in quasi-elastic candidates, for events with one or two vertex tracks, and measured Q^2 between 0.1 and 1 (GeV/c)^2. Right: Significance of the difference between Q^2 from the quasi-elastic hypothesis and Q^2 from the final state energy, for quasielastic candidates with measured Q^2 above 1 GeV^2.

The energy of the proton for the high-Q^2 sample (where the proton almost always interacts) is reconstructed calorimetrically with an expected fractional energy resolution of $35\%/\sqrt{E_{proton}}$.

Although muons are identified by requiring a single long track, no attempt was made (in this initial analysis) to improve particle identification by requiring a dE/dx consistent with the muon or proton tracks. This requirement should be particularly effective for protons of $\mathcal{O}(1)$ GeV momentum[2], and such a requirement can be imposed to optimize the analysis in the future. In addition, it may be possible to improve the efficiency by allowing a shorter muons, with a dE/dx requirement, without sacrificing purity.

If a quasi-elastic interaction is assumed, one can reconstruct the event kinematics from only the momentum and direction of the final state μ. Neglecting the binding energy of the final-state proton,

$$E_\nu^{QE} = \frac{M_N E_\mu - \frac{m_\mu^2}{2}}{M_N - E_\mu + p_\mu \cos\theta_\mu}.$$

If a proton track is identified and its angle and energy are also measured, one can additionally require consistency with the quasi-elastic hypothesis. Two constraints are possible, one on the x of the reconstructed interaction and one on the total p_T of the observed final state.

If the interaction is truly quasi-elastic, then $x = 1$, and therefore $Q^2 = 2M_N\nu$ where ν = E_{had} - M_N, and E_{had} is the energy of the hadronic final state. In this analysis, we test this by comparing Q^2 reconstructed from the lepton kinematics under the quasi-elastic hypothesis to $2M_N\nu$ and forming $(Q^2_\mu - 2M_N\nu)/\sigma$ where the dominant part of the calculated error σ for this term comes from the smearing of hadronic final-state energy. Figure 4 shows the significance of this Q^2 difference for two

[2]See Section **??**.

track quasi-elastic candidates with observed 1 $(GeV/c)^2 < Q^2 < 3$ $(GeV/c)^2$, for quasi-elastic, resonant and deep-inelastic events. This cut can be applied without identifying a proton track if the visible energy, less the muon energy, is assumed to be ν.

The Q^2 significance (x) cut does not use information on the proton direction, and so we impose a second kinematic cut on the total transverse momentum p_T relative to the incoming neutrino direction. This selection requires that a proton track is identified, and we cut on the significance of the difference from $p_T = 0$: $p_T^{tot} < 2\sigma_{p_T}$ if $Q^2 < 3$ (GeV/c)^2, and $p_T^{tot} < 3\sigma_{p_T}$ for higher Q^2.

2.1.8 Unfolding the Quasi-elastic Q^2 and E_ν Distributions

We have estimated the increase in the statistical errors due to resolution smearing. The limited resolution of the MINERνA detector smears out the measured values of E_ν and θ_μ and hence Q^2. The cross section plot and form factor plots should be in terms of true E_ν and Q^2. The scheme to unfold these distribution is described in [21], and we will use his notation. The quanity we minimize is

$$\chi^2 = (R\mu - n)V^{-1}(R\mu - n) + \alpha * S[f]$$

where $R_{i,j}$ is the response matrix (i - smeared, j - true); n_i is a vector of the data (smeared distribution); μ_j is vector of the true distribution; V is the covarience matrix of the data, $V_{i,j} = \delta_{i,j} n_i$; $S[f]$ is a regularization function; and α is the regulatization parameter. The χ^2 is minimized using Minuit by varing μ_j, the unfolded distribution. The unfolded error increase is the "minos" error in Minuit divided by the unsmeared errors. Without $S[f]$, the solution is $\mu = R^{-1}n$. However, this solution does not give the best answer, as the answer tends to oscillate around. The regularization function, $S[f]$, is added the χ^2 to dampen the oscillations, since physics distributions are supposed to be smooth. This function introduces a bias in the unfolding which one makes smaller than the final statistical error. We use $S[f]$ = sum of $(f''(x))^2 \Delta x$, where f is the true distribution, and Δx is the bin width. Given a unfolded histogram, we determine f with spline fit.

For quasi-elastic events the energy and Q^2 can be calculated from just the muon energy and angle. One can show:

$$\Delta Q^2/Q^2 = (1 + E_\nu/E_\mu)(\Delta E_\mu/E_\mu) + (E_\nu/E_\mu) cot(\theta/2)\Delta\theta$$

$$\Delta E_\nu/E_\nu = (E_\nu/E_\mu)(\Delta E_\mu/E_\mu) + (E_\mu/m) sin(\theta)\Delta\theta$$

and with $E_\nu/E_\mu \sim 1.15$:

$$\Delta Q^2/Q^2 = 2.15(\Delta E_\mu/E_\mu) + 1.15 cot(\theta/2)\Delta\theta$$

$$\Delta E_\nu/E_\nu = 1.15(\Delta E_\mu/E_\mu) + (E_\mu/m) sin(\theta)\Delta\theta$$

For this unfolding result, the muon momentum smearing is given used as 5% for $E_\mu < 10GeV$ (for rangeout measurement) and 15% $E_\mu > 10GeV$ (for MINOS magnetic spectrometer measurement). The ΔE_μ terms dominate the smearing as $\Delta\theta \sim .009$. Using the above techniques, we determine the increase in statistical error due to unfolding the smeared distributions.'

2.1.9 Results

Table 1 shows the efficiency and purity of the quasi-elastic sample for different Q^2 bins after each cut. Using these efficiencies and purities, we have determined uncertainties on F_A including efficiency and background effects.

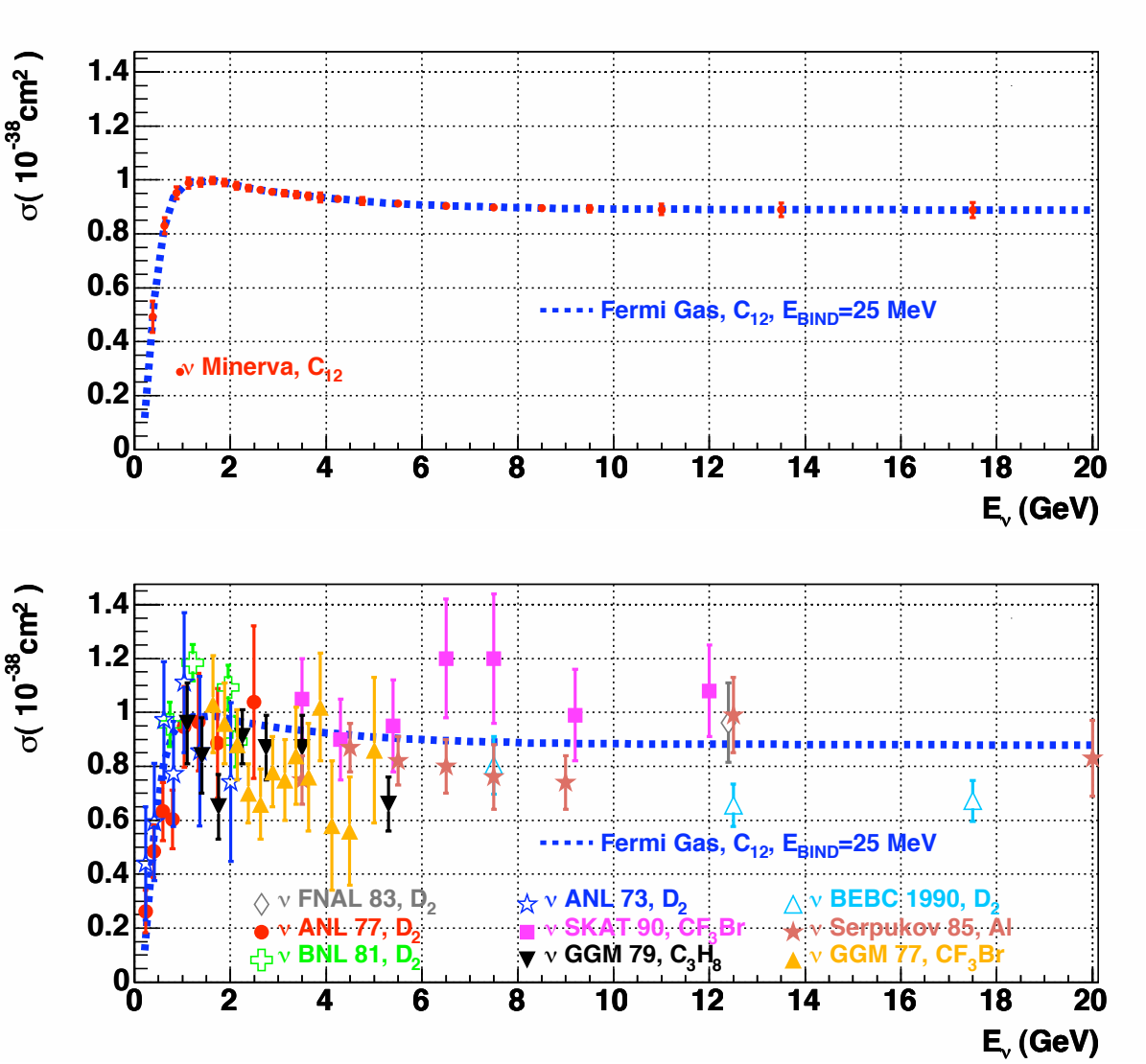

Figure 5: The quasi-elastic neutrino cross-section along with data from various experiments. Representative calculations are shown using BBA-2003 form-factors with $M_A = 1.00$ GeV/c^2. The dashed curve [9] uses a Fermi gas model for carbon with 25 MeV binding energy and 220 MeV/c Fermi momentum. The predicted MINERνA points, with errors, are shown. The data shown in the bottom plot are from FNAL 1983 [11], ANL 1977 [12], BNL 1981 [13], ANL 1973 [14], SKAT 1990 [15], GGM 1979 [16], BEBC 1990 [17], Serpukov 1985 [18], and GGM 1977 [19]. The data have large errors and are only marginally consistent throughout the E_ν range.

	μ		$(Q^2_\mu - 2M\nu)$/err		p_T /err		Hits	
Q^2 bin	Effic	Purity	Effic	Purity	Effic	Purity	Effic	Purity
0.1-0.5	0.926	0.246	0.918	0.442	0.866	0.559	0.775	0.842
0.5 - 1	0.775	0.199	0.765	0.410	0.624	0.486	0.528	0.685
1 - 2	0.600	0.199	0.541	0.416	0.397	0.555	0.338	0.598
2 - 3	0.456	0.146	0.400	0.375	0.344	0.554	0.278	0.676
3 - 10	0.689	0.123	0.600	0.310	0.467	0.420	0.311	0.700

Table 1: Efficiency and purity in Q^2 bins for quasi-elastic candidates

Figure 5 shows predictions for the cross-section assuming the BBA-2003 form-factors, with $M_A = 1.00$ (GeV/c)^2. The predicted MINERνA points are shown along with their expected errors. The MIPP experiment will measure particle production off the NuMI target, and from this, we expect an additional overall uncertainty of 4% from the flux. Figure 5 summarizes current knowledge of neutrino quasi-elastic cross-sections. Among the results shown, there are typically 10–20% normalization uncertainties from knowledge of the fluxes. This plot shows that existing measurements have large errors throughout the E_ν range accessible to MINERνA and especially in the threshold regime crucial to future oscillation experiments.

Figure 6 shows the expected values and errors of F_A in bins of Q^2 for the MINERνA active carbon target, after a four-year exposure in the NuMI beam. The method to extract F_A from $d\sigma/dq^2$ is given in [22]. Clearly the high-Q^2 regime, which is inaccessible to K2K, MiniBooNE and T2K, will be well-resolved in MINERνA. Figure 6 shows these results as a ratio of F_A/F_A(Dipole), demonstrating MINERνA's ability to distinguish between different models of F_A. We effectively show the three different models (described earlier) for F_A as a function of Q^2 . Model 3 (based on duality) is a factor of 1.4 higher than the dipole approximation. Note that resolution effects are included in understanding the statistical error in this extraction of F_A,

Figure 6 shows the extraction of F_A from Miller, Baker, and Kitagaki, using their plots of $d\sigma/dq^2$. For $Q^2 > 2$ (GeV/c)^2 there is essentially no measurement of F_A. Even the measurements of $F_A(Q^2)$ below 2 (GeV/c)^2 have significant errors, hence one cannot assume F_A is a dipole for low Q^2. The maximum Q^2 values that can be achieved with incident neutrino energies of 0.5, 1.0, 1.5 and 2 GeV are 0.5, 1.2, 2.1 and 3.0 (GeV/c)^2, respectively. Since K2K, MiniBooNE, and T2K energies are in the 0.7–1.0 GeV range, these experiments probe the low $Q^2 < 1$ (GeV/c)^2 region where nuclear effects are large (see Figures 7). The low-Q^2 ($Q^2 < 1$ (GeV/c)^2) MiniBooNE and K2K experiments have begun to investigate the various nuclear effects in carbon and oxygen. However, higher Q^2 data are only accessible in experiments like MINERνA, which can span the 2–8 GeV neutrino energy range. MINERνA's measurement of the axial form-factor at high Q^2 will be essential to a complete understanding of the vector and axial structure of the neutron and proton.

2.1.10 Fermi gas model

There are three important nuclear effects in quasi-elastic scattering from bound targets: Fermi motion, Pauli blocking, and corrections to the nucleon form-factors due to distortion of the nucleon's size and its pion cloud in the nucleus. Figure 7 shows the nuclear suppression versus E_ν from a NUANCE[23] calculation[9] using the Smith and Moniz[24] Fermi gas model for carbon. This nuclear model includes Pauli blocking and Fermi motion but not final state interactions. The Fermi gas model uses a nuclear

binding energy $\epsilon = 25$ MeV and Fermi momentum $k_f = 220$ MeV/c. Reference [24] shows how the effective k_f and nuclear potential binding energy ϵ (within a Fermi-gas model) for various nuclei is determined from electron scattering data.

2.1.11 Bound nucleon form-factors

The predicted distortions of nucleon form-factors due to nuclear binding are can be as large as 10% at $Q^2 = 1$ (GeV/c)^2 to 15% at $Q^2 = 2$ (GeV/c)^2. With carbon, iron and lead targets, MINERνA can compare measured form-factors for a range of light to heavy nuclei. Figure 5 shows the cross-section suppression due to bound form-factors. As is described in [10], these effects can cause variations up to 10% in the differential cross-sections at MiniBooNE, K2K and T2K energies.

Requiring vector and axial contributions to W_1 be equal for $Q^2 > 0.5$ (GeV/c)^2 introduces further suppression at low Q^2. Changing the various assumptions in $d\sigma/dq^2$ as calculated with dipole form-factors introduces 5–10% effects on the Q^2 distributions these experiments will see.

2.1.12 Intra-nuclear rescattering

In neutrino experiments, detection of the recoil nucleon helps distinguish quasi-elastic scattering from inelastic reactions. Knowledge of the probability for outgoing protons to reinteract with the target remnant is therefore highly desirable. Similarly, quasi-elastic scattering with nucleons in the high-momentum tail of the nuclear spectral function needs to be understood. More sophisticated treatments than the simple Fermi gas model are required. Conversely, inelastic reactions may be misidentified as quasi-elastic if a final-state pion is absorbed in the nucleus. With its constrained kinematics, low-energy neutrino-oscillation experiments use the quasi-elastic channel to measure the (oscillated) neutrino energy spectrum at the far detector; uncertainty in estimation of non-quasi-elastic background due to proton intra-nuclear rescattering is currently an important source of systematic error in K2K.

The best way to study these effects is to analyze electron scattering on nuclear targets (including the hadronic final states) and test the effects of the experimental cuts on the final-state nucleons. MINERνA can address proton intra-nuclear rescattering by comparing nuclear binding effects in neutrino scattering on carbon to electron data in similar kinematic regions. Indeed, MINERνA members will be working with the CLAS collaboration to study hadronic final states in electron scattering on nuclear targets using existing JLab Hall B data. This analysis will allow theoretical models used in both electron and neutrino experiments to be tested. Other work in progress, with the Ghent nuclear physics group, will develop the theoretical tools needed to extract the axial form-factor of the nucleon using MINERνA quasi-elastic data on carbon. The ultimate aim is to preform nearly identical analyses on both neutrino and electron scattering data in the same range of Q^2.

References

[1] C.H. Llewellyn Smith, Phys. Rep. 3C (1972).

[2] J. Arrington, nucl-ex[0305009].

[3] M. K. Jones *et al.*, Phys. Rev. Lett, 84, (2000) 1398 ; O. Gayou *et al.*, Phys. Rev. Lett, 88 (2002) 092301.

[4] J.J. Kelly, Phys. Rev. C70 (2004) 068202.

[5] R. Bradford, et al., hep[ex0602017].

[6] H. Budd, A. Bodek and J. Arrington, hep-ex[0308005].

[7] R. F. Wagenbrunn *et al.*, hep-ph[0212190].

[8] V. Bernard, L. Elouadrhiri, U.G. Meissner, J.Phys.G28 (2002), hep-ph[0107088].

[9] G. Zeller, private communication.

[10] K. Tsushima, Hungchong Kim, K. Saito, hep-ph[0307013].

[11] T. Kitagaki *et al.*, Phys. Rev. D26 (1983) 436.

[12] S.J. Barish *et al.*, Phys. Rev. D16 (1977) 3103.
BNL D2

[13] N.J. Baker *et al.*, Phys. Rev. D23 (1981) 2499.

[14] W.A. Mann *et al.*, Phys. Rev. Lett. 31 (1973) 844.

[15] J. Brunner *et al.*, Z. Phys. C45 (1990) 551.

[16] M. Pohl *et al.*, Lett. Nuovo Cimento 26 (1979) 332.

[17] D. Allasia *et al.* Nucl. Phys. B **343** (1990) 285

[18] S.V. Belikov *et al.*, Z. Phys. A320 (1985) 625.

[19] S. Bonetti *et al.*, Nuovo Cimento 38 (1977) 260.

[20] K.L. Miller *et al.*, Phys. Rev. D26 (1982) 537.

[21] Glen Cowan, Statistical Data Analysis, Oxford Clarendon Press (1998)

[22] H. Budd, A. Bodek and J. Arrington, hep-ex[0410055].

[23] D. Casper, Nucl. Phys. Proc. Suppl. 112 (2002) 161.

[24] R.A. Smith and E.J. Moniz, Nucl. Phys. B43 (1972) 605.

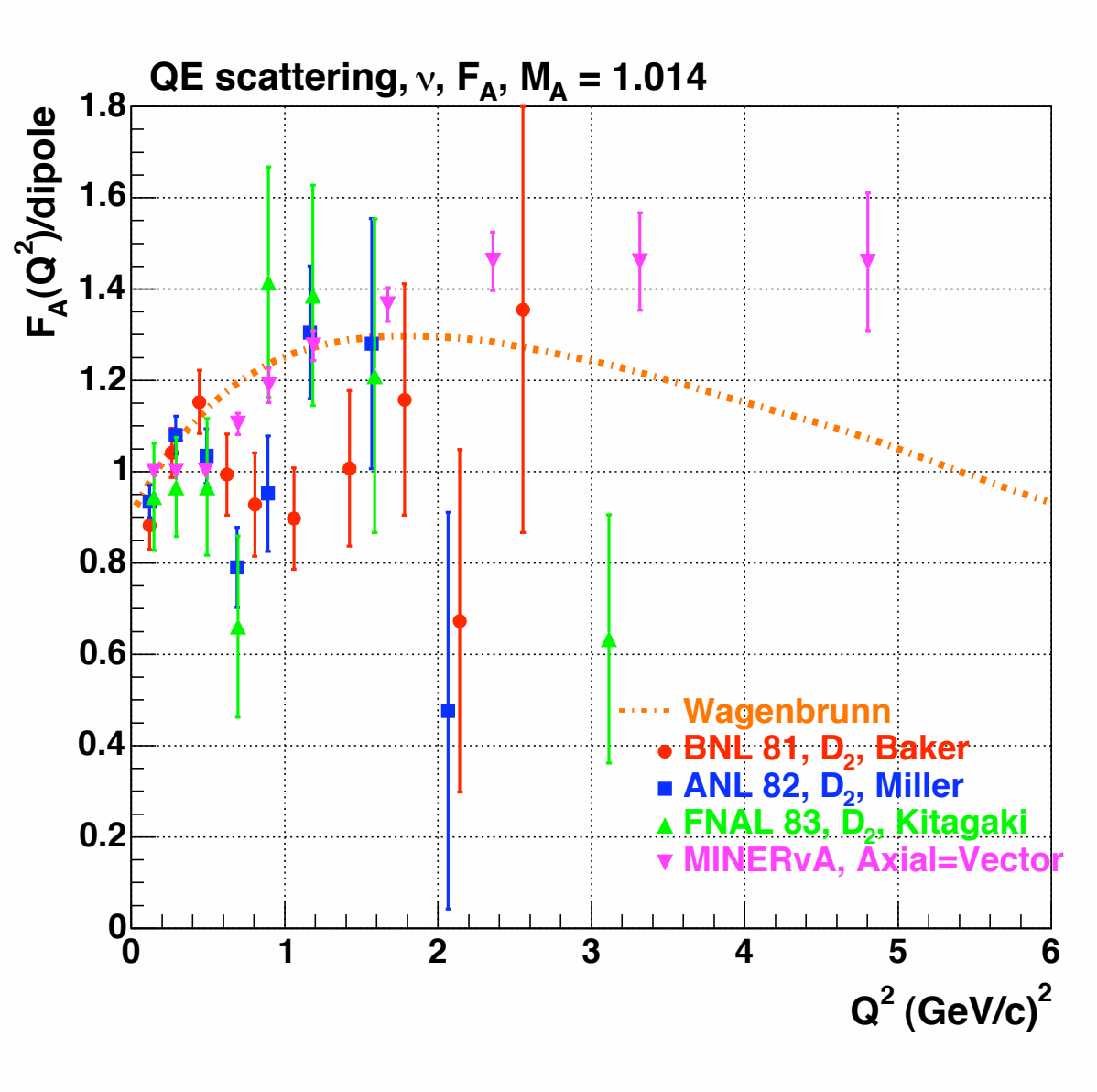

Figure 6: Estimation F_A/dipole for a four year MINERνA run using the quasielastic analysis described in the text. The MINERνA points are plotted assume the Model 3 axial form-factor. Also shown is F_A extracted from deuterium bubble chamber experiments using the $d\sigma/dq^2$ from the papers of FNAL 1983 [11] BNL 1981 [13], and ANL 1982 [20]. Also shown is the expectations from Model 2 for the axial form-factor.

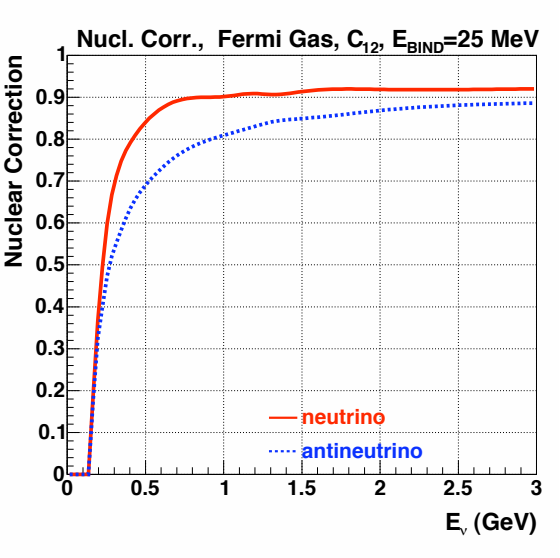

Figure 7: Pauli suppression in a Fermi gas model for carbon with binding energy $\epsilon = 25$ MeV and Fermi momentum $k_f = 220$ MeV/c. A similar suppression is expected for quasi-elastic reactions in MINERνA.